

Probing Magnetic Sublattices in Multiferroic $\text{Ho}_{0.5}\text{Nd}_{0.5}\text{Fe}_3(\text{BO}_3)_4$ Single Crystal using X-ray Magnetic Circular Dichroism

Mikhail Platonov,^{1,2,*} Natalia Kazak,¹ Viacheslav Dudnikov,¹ Fabrice Wilhelm,² Amir Hen,² Vadim Diadkin,² Iurii Dovgaliuk,² Alexey Bosak,² Vladislav Temerov,¹ Irina Gudim,¹ Yurii Knyazev,¹ Sergey Gavrilkin,³ Andrei Rogalev,² and Sergei Ovchinnikov¹

¹*Kirensky Institute of Physics, Federal Research Center KSC SB RAS,
Akademgorodok 50, bld. 38, 660036 Krasnoyarsk, Russia*

²*ESRF-The European Synchrotron, 71 Avenue des Martyrs CS40220, F-38043 Grenoble Cedex 9, France.*

³*P.N. Lebedev Physical Institute of RAS, 119991 Moscow, Russia*

Using element-specific X-ray magnetic circular dichroism (XMCD) technique we have studied different magnetic sublattices in a multiferroic $\text{Ho}_{0.5}\text{Nd}_{0.5}\text{Fe}_3(\text{BO}_3)_4$ single crystal. The XMCD measurements at the $L_{2,3}$ -edges of Ho and Nd, and at the Fe K -edge have been performed at $T=2$ K under a magnetic field up to 17 T applied along the trigonal c -axis as well as in the basal ab -plane. All three magnetic sublattices are shown to undergo a spin-reorientation transition under magnetic field applied along the c -axis. On the contrary, when magnetic field is applied in the ab -plane only the holmium atoms exhibit a magnetization jump. Thus, the element-specific magnetization curves revealed the Ho sublattice to be much stronger coupled to the Fe one than the Nd sublattice. The results demonstrate that the Ho^{3+} subsystem plays even more dominant role in magnetic behavior of $\text{Ho}_{0.5}\text{Nd}_{0.5}\text{Fe}_3(\text{BO}_3)_4$ crystal than in pure $\text{HoFe}_3(\text{BO}_3)_4$ crystal.

PACS numbers: 75.50.Ee, 75.30.Gw, 75.85.+t.

I. INTRODUCTION

The rare-earth ferrobates $\text{ReFe}_3(\text{BO}_3)_4$ (Re - rare earth) crystallize in noncentrosymmetrical trigonal $R\bar{3}2$ or $P3_1(2)21$ space groups, that makes them systems with the coexistence of magnetic order and electric polarization. These materials have been extensively studied since 1970s mainly due to their large magnetoelectric¹⁻⁹, non-linear optical^{10,11} and chiral effects¹².

The crystal structure of ferrobates is affected by the rare-earth ion radius leading the structural transition from the $R\bar{3}2$ to the $P3_121$ structure for the compounds with a smaller Re ionic radii (e.g. Re - Ho, Gd, Tb)^{13,14}. The magnetic structure is such that the helicoidal chains formed by edge-shared FeO_6 octahedra are propagated along the c -axis. The magnetic coupling between Fe ions within a single chain is realized through common oxygen atoms with the coupling angle of $\text{Fe-O-Fe} \approx 100^\circ$. The exchange interaction between nearest magnetic chains takes place via iron-oxygen-rare-earth (Fe-O-Re-O-Fe) ($d_{\text{Fe-Fe}} = 3.76$ Å) and iron-oxygen-boron Fe-O-B-O-Fe ($d_{\text{Fe-Fe}} = 4.83$ Å) pathways. The rare-earth ions are located in a prisms ReO_6 , with the inter-ionic distance $d_{\text{Re-Re}} \sim 6$ Å. The iron subsystem is antiferromagnetically ordered at $T_N = 30\text{-}40$ K. The f - f exchange interaction is weak ($J^{\text{Re-Re}}/k_B < 1$ K) compared with the $J_{\text{Fe-Fe}}$. The magnetic order in both Re and Fe subsystems occurs simultaneously due to the f - d exchange interaction. Furthermore, depending on the type of Re ion, both the easy-plane (EP) and easy-axis (EA) types of magnetic anisotropy can be realized¹⁵⁻¹⁷.

In this study, we focused on the $\text{Ho}_{0.5}\text{Nd}_{0.5}\text{Fe}_3(\text{BO}_3)_4$ single crystal, which is distinguished by its magnetic and magnetoelectric properties from the pure $\text{HoFe}_3(\text{BO}_3)_4$ and $\text{NdFe}_3(\text{BO}_3)_4$ compounds. The magnetic struc-

tures of $\text{HoFe}_3(\text{BO}_3)_4$ and $\text{NdFe}_3(\text{BO}_3)_4$ were studied using neutron scattering, and resonant/non-resonant magnetic X-ray scattering¹⁸⁻²². In $\text{NdFe}_3(\text{BO}_3)_4$ the magnetic anisotropy of Nd^{3+} ions stabilizes the EP magnetic structure with $T_N = 31$ K, while in $\text{HoFe}_3(\text{BO}_3)_4$ ($T_N = 38$ K) the competition between the contributions of holmium and iron sublattices induces the spontaneous spin-reorientation transition from the high-temperature EP to low-temperature EA states at $T_{SR} = 5$ K. The substitution of 50% Ho^{3+} ions by Nd^{3+} ions leads to the stabilization of the EA phase and the increase in temperature of the spin-reorientation transition up to $T_{SR} = 9$ K¹⁵. The field-induced spin-reorientation (spin-flop) transitions observed in the parent compounds are shifted to the high-field region: from ~ 0.6 T to 1 T for the parallel direction and from ~ 0.9 T to 2.3 T for the perpendicular direction of magnetic field relative trigonal c -axis (Fig. 1).

Moreover, the $\text{HoFe}_3(\text{BO}_3)_4$ crystal exhibits a zero-field spontaneous electrical polarization (~ 80 $\mu\text{C}/\text{m}^2$) below T_N , which is suppressed by the external magnetic fields¹⁵. $\text{NdFe}_3(\text{BO}_3)_4$ in turn has a much larger (above 300 $\mu\text{C}/\text{m}^2$) electric polarization controlled by the magnetic field and the giant quadratic magnetoelectric effect¹. Most interestingly, the solid solution of $\text{Ho}_{0.5}\text{Nd}_{0.5}\text{Fe}_3(\text{BO}_3)_4$ combines the main features observed in the end members: the zero-field spontaneous polarization, which diminishes in the magnetic fields along the c -axis similar to $\text{HoFe}_3(\text{BO}_3)_4$; and the large value of the polarization (up to 900 $\mu\text{C}/\text{m}^2$ at 7 T) induced by the magnetic fields along the a -axis exceeding that in $\text{NdFe}_3(\text{BO}_3)_4$. The $\text{Ho}_{0.5}\text{Nd}_{0.5}\text{Fe}_3(\text{BO}_3)_4$ thus demonstrates complex behavior of the temperature and field dependences of the electric polarization¹⁵. The sign reversals of the polarization and steplike anomalies

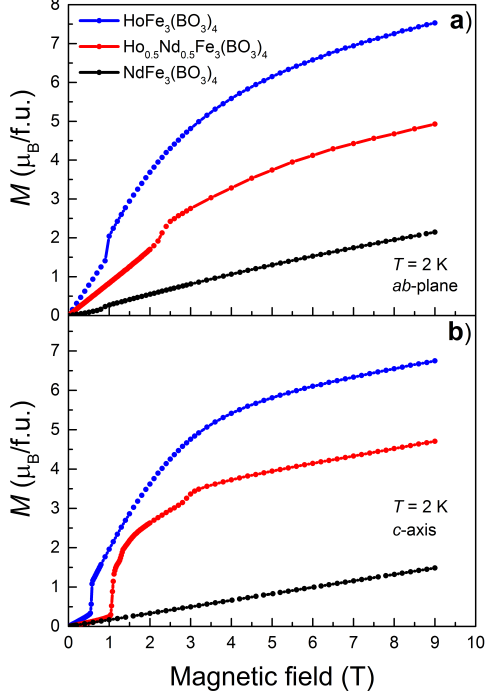


FIG. 1. (Color online) (a) Field dependences of the magnetizations for $\text{Ho}_{1-x}\text{Nd}_x\text{Fe}_3(\text{BO}_3)_4$ ($x = 0.0, 0.5, 1.0$) for the applied magnetic field in basal ab -plane (a) and trigonal c -axis (b), $T = 2$ K.

correlate with the features at the magnetization curves as shown in the Figure 2. The magnetoelectric effect in $\text{Ho}_{0.5}\text{Nd}_{0.5}\text{Fe}_3(\text{BO}_3)_4$ is therefore likely to be associated with a spin-reorientation transitions in external magnetic fields.

To elucidate a possible relation of this behavior to rare-earth and iron magnetism, a systematic study of the element-specific magnetization has been undertaken. The presence of the three magnetic subsystems in $\text{Ho}_{0.5}\text{Nd}_{0.5}\text{Fe}_3(\text{BO}_3)_4$ makes this compound an interesting object for the element-specific XMCD study. Our data show that if the magnetic field is applied along the c -axis all three (Ho, Nd and Fe) magnetic sublattices undergo the spin-reorientation transition at $H_{sf}^c = 1$ T, with the dominant changes in the holmium one. This demonstrates the existence of the magnetic coupling between them. For the applying magnetic field in the ab -plane it is only holmium magnetic moment that shows the jump. The Ho^{3+} ions are responsible for the easy-axis magnetic anisotropy inducing spin-flop transitions in the Fe^{3+} and Nd^{3+} sublattices, and participate in the strong magnetic coupling with the Fe^{3+} subsystem. The obtained results show the success in the disentangling of the magnetic contributions of different sublattices in the multiferroic ferroborate.

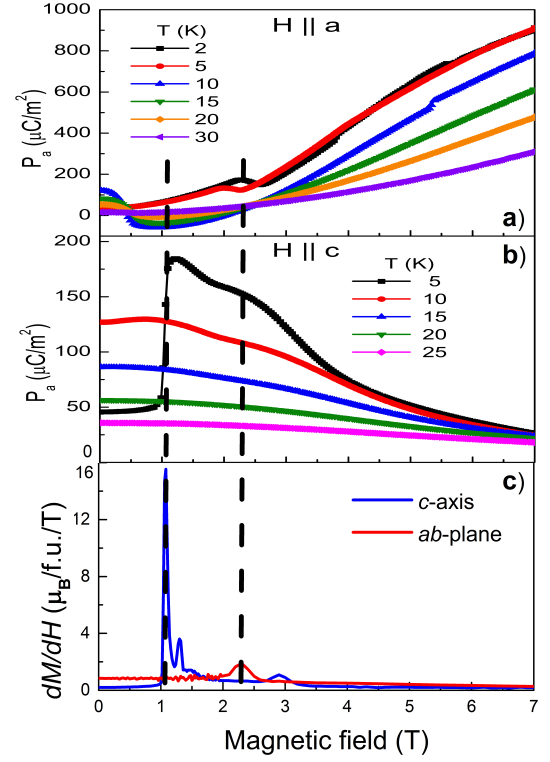


FIG. 2. (Color online) Magnetic-field dependence of the polarization P_a at different temperatures. a) $H \parallel a$ axis, b) $H \parallel c$ -axis [data taken from Fig.15¹⁵], c) the derivatives dM/dH obtained using the magnetic data of Fig. 1, which show the onset of spin-flop transitions as a function of applied field ($T = 2$ K). The dashed lines denote the correlation between the spin-flop transitions and the features of the electrical polarization of $\text{Ho}_{0.5}\text{Nd}_{0.5}\text{Fe}_3(\text{BO}_3)_4$.

II. EXPERIMENTAL TECHNIQUES

To perform the experiments the $\text{Ho}_{1-x}\text{Nd}_x\text{Fe}_3(\text{BO}_3)_4$ single crystals with a size of 5-7 mm were grown from melt solutions based on bismuth trimolibdate¹⁵. The single crystals had a high optical quality, a green color typical for ferroborates, and natural facets. From these crystals, oriented plates were cut, grounded to a thickness of 1-2 mm, and finally polished using diamond powder of 0.25 micron. The crystallographic orientations were identified by a series of X-ray diffraction experiments at the BM01A endstation of the Swiss-Norwegian and ID28 beamlines at the ESRF. The crystal structure of $\text{Ho}_{0.5}\text{Nd}_{0.5}\text{Fe}_3(\text{BO}_3)_4$ was investigated up to 100 K without detecting any sign of a structural transition. The ratio between enantiomeric twin components for racemic $\text{Ho}_{0.5}\text{Nd}_{0.5}\text{Fe}_3(\text{BO}_3)_4$ crystal was determined. The refined value of the Flack parameter for $\text{Ho}_{0.5}\text{Nd}_{0.5}\text{Fe}_3(\text{BO}_3)_4$ at 0.68 Å is 0.27(6). The room temperature lattice parameters are $a=9.57280(10)$ Å, $b=9.57280(10)$ Å, $c=7.58760(10)$ Å, $\alpha=\beta=90.00^\circ$, $\gamma=120.00^\circ$, $V=602.161(15)$ Å³, vary almost linearly with

Nd content and are in good agreement with previous published data^{18,22}.

Next the low-temperature macroscopic magnetization measurements in $\text{Ho}_{1-x}\text{Nd}_x\text{Fe}_3(\text{BO}_3)_4$ ($x = 0.0, 0.5, 1.0$) single crystals as a function of applied magnetic fields up to 9 T (Fig. 1) were performed using a commercial Physical Property Measurement System (PPMS) from Quantum Design using the Vibrating Sample Magnetometry (VSM) configuration. The magnetization was measured under an external magnetic field applied parallel and perpendicular to the samples' trigonal c -axis.

Element-specific XANES and XMCD measurements were then carried out at the Fe K - (7112 eV), Ho $L_{3,2}$ - (8071, 8919 eV), and Nd $L_{3,2}$ - (6208, 6722 eV) absorption edges at the ESRF ID12 beamline²³. The APPLE-II undulator and a Si(111) double crystal monochromator were used to collect the spectra at the respective energies. The samples were glued to the sample holder with Apiezon grease. The measurements were done below the spin-reorientation transition at $T = 2$ K. The single crystal was oriented such that the trigonal c -axis was parallel and perpendicular to x-ray wave-vector, since x-rays and applied magnetic field are collinear. The XMCD signal was obtained by differences of XANES spectra measured with opposite helicities of the incoming photons at a fixed magnetic field value up to ± 17 T. The beam size was approximately $200 \mu\text{m}$, and for each helicity the 24 spectra were recorded and averaged. No radiation damage of the sample was detected. All spectra were measured using the total fluorescence yield detection mode in "backscattering" geometry resulting in the bulk sensitive information. The XMCD spectra at the Fe K - and Ho/Nd $L_{3,2}$ -edges were normalized to the corresponding edge jump of the absorption spectrum. The element-specific magnetization curves were obtained by the measurement of XMCD signal as a function of the field at a fixed energy.

III. RESULTS

XANES and XMCD spectra at the Fe K -edge are shown in Fig. 3a. The overall shape of the XMCD signal is interesting. Three spectral energy regions can be identified: a pre-edge region, a rising edge, and a main absorption band. The small double-peak structure between 7110 and 7120 eV is observed in the pre-edge region. The shoulder (7122 eV) in normal incidence is assigned to $1s-4p$ of Fe hybridized with $2p_z$ states of the O ligands²⁴. Other maxima of the absorption curve in the main absorption band correspond to the transitions to continuum states of p -character and are very sensitive to the relative positions of the atoms. A clear dichroic signal can be observed near the edge with the maximum of the order of $8 \cdot 10^{-4}$ of the edge jump for Fe. The XMCD K -edge spectrum is mostly dominated by the excitation of a $1s$ electron to unoccupied $4p$ states. Since the signal is nonzero, it reflects the magnetic polarization of the Fe $4p$ band caused by the intra-atomic exchange interac-

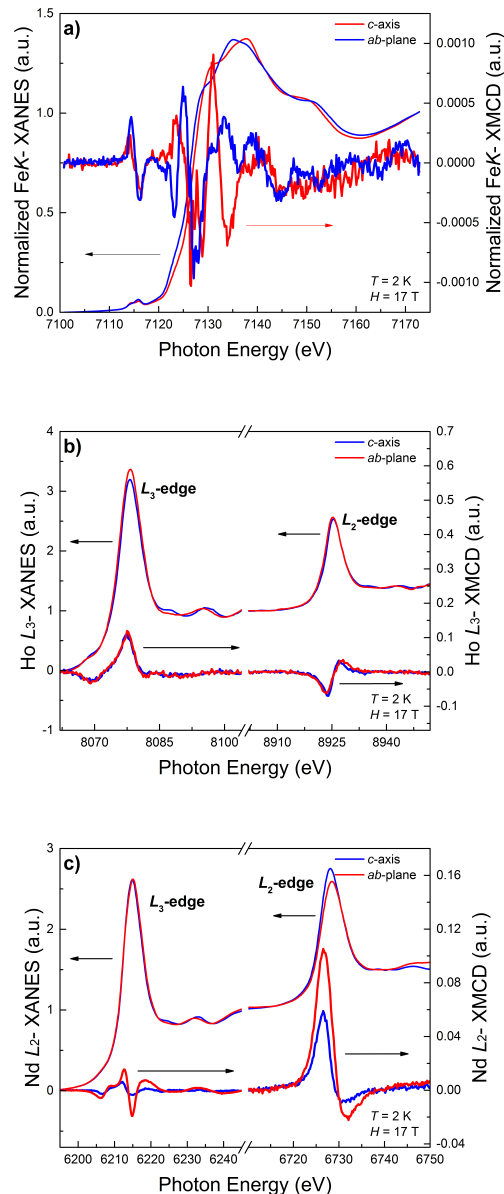


FIG. 3. (Color online) Normalized XANES/XMCD spectra recorded at 2 K and 17 T for $\text{Ho}_{0.5}\text{Nd}_{0.5}\text{Fe}_3(\text{BO}_3)_4$ for different orientations of wave vector k relative trigonal c -axis: a) Fe K -edge; b) Ho $L_{3,2}$ -edges; c) Nd $L_{3,2}$ -edges.

tion with the $3d$ band. So, the Fe K -edge XMCD signal is proportional to the magnetization of the $3d$ states. The probing depth at the K -edge is considerably larger than the escape depth of electrons that are usually used for detection of X-ray absorption and XMCD spectra at the $L_{3,2}$ -edges of $3d$ transition metals. Accordingly, the present data are representative of the bulk, that is of importance to a study of magnetic dielectric oxides.

XANES and XMCD spectra collected at the Ho and Nd $L_{3,2}$ -edges are shown in Fig. 3b and 3c respectively. The Ho and Nd XANES spectra were normalized to one

at the L_3 - and half at the L_2 -edge to reflect the 2:1 ratio of the initial state at these edges ($2p_{3/2}$ and $2p_{1/2}$, respectively). Each of these spectra can be decomposed into three main features: the first corresponds to $2p \rightarrow 5d$ electronic transitions; second, a steplike edge feature that is associated with $2p \rightarrow$ continuum electronic excitations; and, third, a series of smaller "fine structure" oscillations that arise from the backscattering of photoelectrons by neighboring atoms. Dipolar selection rules make the magnetic signal at the rare-earth $L_{3,2}$ -absorption edges sensitive to the spin polarization of the intermediate $5d$ level as a result of a $4f$ - $5d$ exchange interaction²⁵.

The XMCD signal obtained across the two edges shows different intensities with a strong dichroic magnetic signal. The L_3 -edges XMCD spectra of both Ho and Nd consist of a negative dip followed by a main positive peak above the Fermi energy. Such a negative dip is very small for the Nd case. This spectral feature has been associated to a quadrupolar transition ($2p \rightarrow 4f$) that should be present at the L_3 -edge spectra of heavy rare-earth and its magnitude is small for light lanthanide, i.e. Nd^{26,27}. The Ho L_2 -edge XMCD spectra consists of a main negative peak above the edge and a smaller positive peak at higher energy. The amplitude of the L_2 -edge XMCD spectra decreases from Ho to Nd as well. We can assume that the Ho moments in the $\text{Ho}_{0.5}\text{Nd}_{0.5}\text{Fe}_3(\text{BO}_3)_4$ sample are polarized in the direction of applied field, as follows from the positive L_3 - and negative L_2 -peaks^{26,27}.

It is important to note that the evolution with the field of the XMCD signal at the $L_{3,2}$ -edges can be considered directly proportional to the local magnetization from the $3d$ or $4f$ states. The specific energies that correspond to the maximum amplitude of the XMCD signals at the L_3 -edge of Ho ($E_{\text{Ho}}^{L_3} = 8077.13$ eV), and the K -edge of Fe ($E_{\text{Fe}}^K = 7124.83$ eV) were selected. Due to the small value of the XMCD signal at L_3 -edge of Nd, the L_2 -edge was selected for XMCD measurement ($E_{\text{Nd}}^{L_2} = 6726.16$ eV). The element-specific magnetization curves of $\text{Ho}_{0.5}\text{Nd}_{0.5}\text{Fe}_3(\text{BO}_3)_4$ at the Fe K -, as well as at the Ho, Nd $L_{3,2}$ -edges in comparison with macroscopic magnetization are shown in Fig. 4. Depending on their direction, the external magnetic fields have a drastic effect on the magnetic behavior of rare-earth and iron sublattices.

Ho L_3 -edge. The field dependence of the Ho L_3 -edge magnetization reveals a sharp increase of the magnetic moment at the critical fields of $H_{sf}^c = 1$ T for applied magnetic field along the trigonal c -axis. The magnetization jump reduces in value, becomes less sharp and is shifted toward higher fields ($H_{sf}^{ab} = 2.2$ T) for magnetic field applied in the basal ab -plane. These jumps are related to the holmium magnetic moments reorientations. In the spin-flop phase ($H < H_{sf}$) there is a linear contribution to holmium magnetization with the initial susceptibility in the basal ab -plane more large than that along c -axis. It is worth noting that the Ho L_3 -edge magnetization obtained from the XMCD data matches well the bulk magnetization measurements at the fields $H < 5$ T and tends to the saturation at larger fields. At the fields $H \sim 6$ T

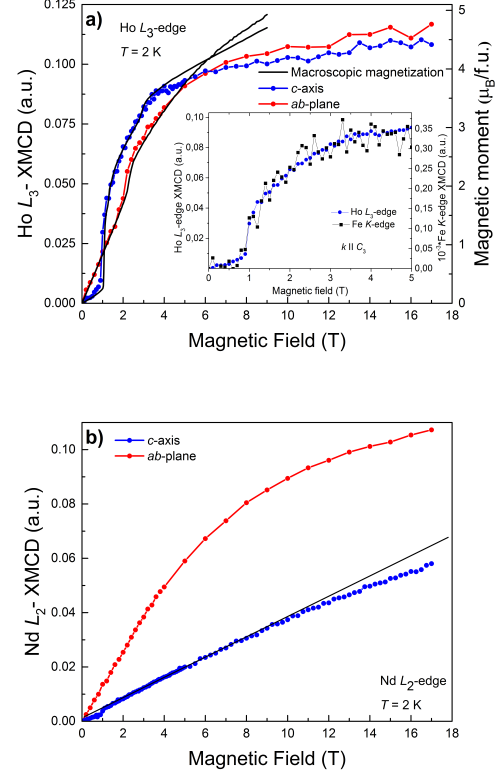


FIG. 4. (Color online) (a) The element-specific magnetization curves of $\text{Ho}_{0.5}\text{Nd}_{0.5}\text{Fe}_3(\text{BO}_3)_4$ as a function of applied field: a) Ho L_3 -edge and bulk magnetization curves. The inset: the comparison of Ho L_3 - and Fe K -edges XMCD magnetization curves for the applied field along c -axis; b) Nd L_2 -edge. The inset shows the linear dependence of the Nd L_2 -edge XMCD magnetization on the applied field along c -axis.

the intersection of the XMCD magnetization curves measured along and perpendicular to the c -axis takes place.

Nd L_2 -edge. The Nd L_2 -edge magnetization shows a strong anisotropy (Fig. 4b). The applying magnetic field along trigonal c -axis causes a visible jump in the magnetization at $H_{sf}^c = 1$ T. There is a linear field dependence of the magnetization for the fields $H_{sf}^c < H < 9$ T and the tendency to the flattening at $H > 9$ T. In contrast, for applied magnetic fields in the basal ab -plane the nonlinear behavior of the magnetization without any features is observed up to highest fields. At magnetic field of 17 T the Nd L_2 -edge XMCD signal in ab -plane is twice of that along c -axis.

Fe K -edge. The Fe K -edge magnetization as a function of the applied field is presented in the inset to Fig. 4a. The Fe K -edge XMCD signal is two orders value smaller than that at Ho L_3 -edge, confirming the antiferromagnetic ordering of Fe^{3+} magnetic moments as presumed from macroscopic magnetization study. The magnetic field applied along the c -axis induces a sharp jump in the iron magnetization at $H_{sf}^c = 1$ T similar that ob-

served for the rare-earth magnetization curves. At the fields above H_{sf}^c the iron magnetization follows to the holmium magnetization and tends to the saturation indicating that these atoms are strongly magnetically coupled. The magnitude of the Fe K -edge XMCD signal in ab -plane is commensurable with that of the noise. For this reason these data does not discussed.

IV. DISCUSSION

For both orientations of the magnetic fields the Ho L_3 -, Nd L_2 -, and Fe K -edge magnetization curves tend to zero as the magnetic field tends to zero. This observation agrees with the assumption of the polarization of rare-earth sublattices by antiferromagnetic interactions with the iron subsystem (Re^{3+} -O- Fe^{3+}). The each of the rare-earth sublattice (Ho and Nd) should be divided into two magnetic sublattices with magnetic moments oriented oppositely. At $T < T_{SR}$ the magnetic moments of all three magnetic sublattices are presumably oriented along trigonal c -axis. For this reason the Fe K -edge magnetization shows very small longitudinal susceptibility prior to the spin-flop transition. As applied field along c -axis increases the contribution of the rare-earth sublattice, the magnetic moment opposed the field is decreased determining the character of the magnetization in the spin-flop phase. At $H_{sf}^c = 1$ T the magnetic moments re-orientation occurs in a jump. The observation of the XMCD magnetizations jumps indicates that a magnetic field applied along c -axis changes the orientations of the magnetic moments of all three magnetic sublattices and primarily concerned the holmium one. If the external field is applied in the basal ab -plane only the Ho L_3 -edge magnetization curve shows the jump at $H_{sf}^{ab} = 2.2$ T.

In the flop phase ($H > H_{sf}$) the holmium and neodymium sublattices magnetizations measured via XMCD have a quite different behaviors. The Ho L_3 -edge magnetization tends to the saturation, demonstrating the small cant angle of the magnetization curve (perpendicular susceptibility). This lack of saturation is probably due to the weak f - d exchange interaction. For the same reason, the magnetic moments of the holmium sublattices undergo the spin-reorientation transition more rapidly than those of the iron sublattices. At the magnetic fields above spin-flop transition the Fe magnetic moments gain a small cant toward the external field direction under the action of the effective magnetic field. It was previously proposed that the f - d exchange interaction does not affect the process of rotation the Fe magnetic moments at the magnetic fields $H > H_{sf}$, giving rise to linear dependence on the field. However, XMCD measurements in $Ho_{0.5}Nd_{0.5}Fe_3(BO_3)_4$ show strong magnetic coupling between the holmium and iron sublattices, which is reflected in the lack of the saturation in the former and the nonlinear behavior of the magnetization in the latter.

The Nd magnetization curves show strong anisotropy, which is manifested in the difference in the magnitudes

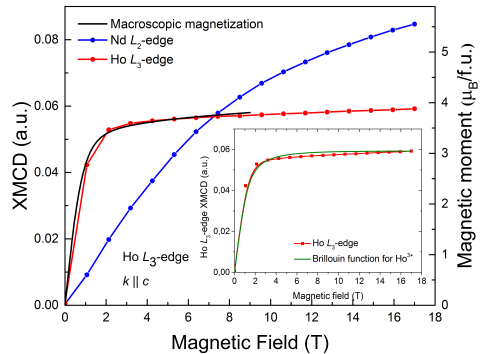


FIG. 5. (Color online) The macroscopic and element-specific magnetization curves of $Ho_{0.5}Nd_{0.5}Al_3(BO_3)_4$ at Ho L_3 - and Nd L_2 -edges as a function of the applied field along c -axis, $T=2$ K. The inset shows the fit using the Brillouin function.

of XMCD signals and in the form of the magnetization curves obtained for two magnetic field orientations. For the applied field in the ab -plane the magnitude of the XMCD signal reaches 0.11 at 17 T and is comparable with that found in permanent magnet $Nd_2Fe_{14}B$ ²⁸. At the same time the Nd XMCD dichroic signal along trigonal c -axis reaches the smaller magnitude of ~ 0.6 . This observed difference reflects the easy-plane anisotropy of Nd^{3+} ion.

The effect of the f - d exchange interaction on the rare-earth sublattices can be studied by measuring the element-specific magnetization curve at Ho L_3 - and Nd L_2 -edges in $Ho_{0.5}Nd_{0.5}Al_3(BO_3)_4$. This compound is paramagnet showing the large magnetoelectric effect $\Delta P \approx 1400 \mu C/m^2$ at 9 T exceeding known values in the ferrobates. The element-specific magnetization curves in $Ho_{0.5}Nd_{0.5}Al_3(BO_3)_4$ measured at trigonal c -axis and at $T=2$ K are shown in Fig. 5. When the Fe ion is replaced by Al ion the amplitude of the XMCD signal at Ho L_3 -edge decreases. Indeed, in the absence of the exchange interaction with the iron subsystem the Ho magnetization curve clearly shows the saturation at fields above 6 T while the Nd magnetization curve monotonically increases up to the highest field. Considering that the XMCD at the rare-earth $L_{3,2}$ -absorption edges is exclusively owing to the rare-earth and is proportional to the $4f$ electrons we can assume that in the case of $Ho_{0.5}Nd_{0.5}Al_3(BO_3)_4$ the Ho and Nd XMCD contributions are close to the free-ion ones. We fitted the Ho L_3 -edge magnetization using the Brillouin function assuming $J=8$ and $g=1.25$ close to free Ho^{3+} ion. The agreement with the XMCD data is quite good with a saturation of ~ 0.06 . However, using the free-ion parameters for the Brillouin function of Nd L_2 -edge magnetization leads to the disagreement. The main difference is that free Ho^{3+} ion with f^{10} configuration has the ground state 5I_8 ($S=2$, $L=6$) separated by $\Delta=5000 \text{ cm}^{-1}$ from the first excited state, while the ground state

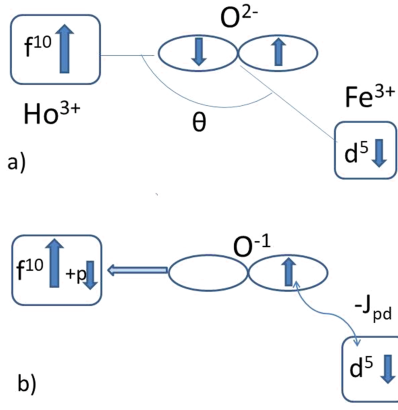


FIG. 6. (Color online) Scheme of the superexchange interaction for $\text{Ho}^{3+}\text{-O}^{2-}\text{-Fe}^{3+}$ chain with the angle θ . a) The initial state. b) the oxygen spin down electron transfers to Ho ion while spin up electron has exchange coupling $-J_{pd}$ with Fe ion spin.

of Nd^{3+} ion with f^3 configuration is ${}^4I_{9/2}$ ($S=3/2$, $L=6$) and is separated by smaller gap of $\Delta \approx 1800 \text{ cm}^{-1}$ from the first excited state ${}^4I_{11/2}$ leading to the admixing to the ground state. The next important finding is the Ho magnetization is well agreed with bulk magnetization indicating the dominant contribution to the magnetism and magnetocrystalline anisotropy of $\text{Ho}_{0.5}\text{Nd}_{0.5}\text{Al}_3(\text{BO}_3)_4$ similar to $\text{Ho}_{0.5}\text{Nd}_{0.5}\text{Fe}_3(\text{BO}_3)_4$.

So, one can conclude that the Ho^{3+} magnetic sublattice is responsible for the spin-reorientation transitions in the $\text{Ho}_{0.5}\text{Nd}_{0.5}\text{Fe}_3(\text{BO}_3)_4$ antiferromagnet and plays a crucial role in the magnetism of the system. The Ho^{3+} magnetic moment determines the direction of the Fe^{3+} and consequently of the Nd^{3+} magnetic moments, causing them to be guided along the trigonal c -axis at low temperatures and involves them to the spin-orientation process. The intersection of the bulk magnetization curves of $\text{Ho}_{0.5}\text{Nd}_{0.5}\text{Fe}_3(\text{BO}_3)_4$ at $\sim 6 \text{ T}$ is similar to that observed at the $\text{HoAl}_3(\text{BO}_3)_4$ and $\text{Ho}_{0.5}\text{Nd}_{0.5}\text{Al}_3(\text{BO}_3)_4$ at $\sim 7.5 \text{ T}$ and was not observed in $\text{HoFe}_3(\text{BO}_3)_4$. This feature is due to the Ho^{3+} magnetic contribution as shown from the XMCD data in Fig. 4a and indicates the qualitative changes of this contribution comparing with $\text{HoFe}_3(\text{BO}_3)_4$ due to the crystal field effect.

The neodymium sublattice coupled by comparatively weak exchange interaction with the iron sublattice undergoes considerably smaller change in the magnetic moment. The effect of the Nd^{3+} magnetic subsystem is mainly manifested in the linear contribution to the macroscopic magnetization along c -axis and in the extra contribution to the magnetization in the ab -plane. To gain insight into the reduction of the neodymium contribution in the $\text{Ho}_{0.5}\text{Nd}_{0.5}\text{Fe}_3(\text{BO}_3)_4$ solid solution estimations of the f - d superexchange interactions are needed. The qualitative analysis of the superexchange interaction for $\text{Ho}^{3+}\text{-O}^{2-}\text{-Fe}^{3+}$ and $\text{Nd}^{3+}\text{-O}^{2-}\text{-Fe}^{3+}$ chains is given below. Following to the Kramers-Anderson model, the

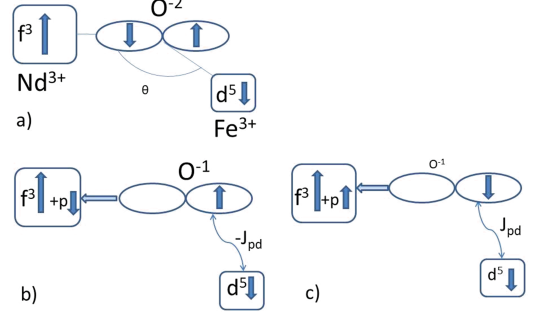


FIG. 7. (Color online) Scheme of the superexchange interaction for $\text{Nd}^{3+}\text{-O}^{2-}\text{-Fe}^{3+}$ chain with the angle θ . a) The initial state. b) The oxygen spin down electron transfers to Nd ion while spin up electron has exchange coupling $-J_{pd}$ with Fe ion spin. c) The oxygen spin up electron transfers to Nd ion while spin down electron has exchange coupling J_{pd} with Fe ion spin.

superexchange interaction for $\text{Ho}^{3+}\text{-O}^{2-}\text{-Fe}^{3+}$ chain with an angle $\theta \sim 120^\circ$ is forming as illustrated in Fig. 6. According to the Pauli principle only spin down oxygen electron can transfer to Ho^{3+} ion with more than half-filled f -shell. The oxygen spin up electron has exchange coupling $-J_{pd}$ with Fe ion spin. For less than half-filled f -shell of Nd^{3+} ion both oxygen electrons with spin up and spin down can transfer to Nd^{3+} ion (Fig. 7). Spin down transferred electron result in $-J_{pd}$ coupling (Fig. 7b), while the oxygen spin up electron transfer result in opposite sign $-J_{pd}$ coupling (Fig. 7c). Thus both spin channels for $\text{Nd}^{3+}\text{-O}^{2-}\text{-Fe}^{3+}$ chain partially compensate each other and resulting superexchange interaction for $\text{Nd}^{3+}\text{-O}^{2-}\text{-Fe}^{3+}$ chain is weaker than for $\text{Ho}^{3+}\text{-O}^{2-}\text{-Fe}^{3+}$ one.

V. CONCLUSIONS

The Fe K -edge, Ho $L_{3,2}$ -edge and Nd $L_{3,2}$ -edge XMCD spectra have been measured at $T=2 \text{ K}$ under magnetic field $\pm 17 \text{ T}$ for the $\text{Ho}_{0.5}\text{Nd}_{0.5}\text{Fe}_3(\text{BO}_3)_4$ single crystal. The external magnetic field was applied along the trigonal c -axis and in the basal ab -plane. It was found, that all three magnetic sublattices undergo spin-reorientation transition at $H_{sf}^c=1 \text{ T}$ if the magnetic field is applied along c -axis, and only holmium subsystem shows the sharp increase of the magnetic moment at $H_{sf}^{ab}=2.2 \text{ T}$ for the applied magnetic field in the ab -plane. The main conclusion of this study is to the Ho and Fe magnetic sublattices are strongly coupled and the magnetic properties including the magnetocrystalline anisotropy in the $\text{Ho}_{0.5}\text{Nd}_{0.5}\text{Fe}_3(\text{BO}_3)_4$ single crystal are due to anisotropy of the Ho sublattice. This conclusion seems unexpected taking into account the significant substitution (50%) of holmium ions by neodymium ones, which have dif-

ferent anisotropy signs. Nevertheless the assumption that the Ho^{3+} ion magnetic anisotropy is enhanced in $\text{Ho}_{0.5}\text{Nd}_{0.5}\text{Fe}_3(\text{BO}_3)_4$ in compare with $\text{HoFe}_3(\text{BO}_3)_4$ can explain the observed stabilization an easy-axis magnetic structure at higher temperature (T_{SR}) and magnetic field (H_{sf}). The spin-flop transitions observed at the macroscopic magnetization curve and associated anomalies of electrical polarization are shown to be due to the Ho^{3+} magnetic moment reorientation from the easy-axis to easy-plane state. The reasons of the electric polarization changes found in $\text{Ho}_{0.5}\text{Nd}_{0.5}\text{Fe}_3(\text{BO}_3)_4$ system relative the parent samples $\text{HoFe}_3(\text{BO}_3)_4$ and $\text{NdFe}_3(\text{BO}_3)_4$ is probably due to the increase in the Ho sublattice con-

tribution as well as to the qualitative changes of this contribution due to the crystal field effect.

ACKNOWLEDGMENTS

The study was supported in part by the grants of the Russian Foundation for Basic Research (project nos. 16-32-60049, 17-02-00826) and the Foundation for Assistance to Small Innovative Enterprises (FASIE, UMNIK program). The authors thank the BM01A/ID28/ID12 beamlines staffs for help during the experiment and also gratefully acknowledge the beamtime provision (proposal HC-1804) by the ESRF.

-
- * ms-platunov@yandex.ru
- ¹ A. K. Zvezdin, G. P. Vorob'ev, A. M. Kadomtseva, Y. F. Popov, A. P. Pyatakov, L. N. Bezmaternykh, and E. A. Popova, JETP letters 83(11), 509-514 (2006).
 - ² K. C. Liang, R. P. Chaudhury, B. Lorenz, Y. Y. Sun, L. N. Bezmaternykh, V. L. Temerov, and C. W. Chu. Physical Review B 83(18), 180417 (2011).
 - ³ A. K. Zvezdin, S. S. Krotov, A. M. Kadomtseva, G. P. Vorob'ev, Y. F. Popov, A. P. Pyatakov, and E. A. Popova, JETP Letters 81(6), 272-276 (2005).
 - ⁴ A. M. Kadomtseva, Y. F. Popov, G. P. Vorobev, A. A. Mukhin, V. Y. Ivanov, A. M. Kuzmenko, and L. N. Bezmaternykh, JETP letters, 87(1), 39-44 (2008).
 - ⁵ A. M. Kadomtseva, Y. F. Popov, G. P. Vorobev, A. P. Pyatakov, S. S. Krotov, K. I. Kamilov, and L. N. Bezmaternykh, Low Temperature Physics, 36(6), 511-521 (2010).
 - ⁶ A. M. Kadomtseva, G. P. Vorobev, Y. F. Popov, A. P. Pyatakov, A. A. Mukhin, V. Y. Ivanov, and L. N. Bezmaternykh, Journal of Experimental and Theoretical Physics, 114(5), 810-817 (2012).
 - ⁷ A. A. Mukhin, G. P. Vorobev, V. Y. Ivanov, A. M. Kadomtseva, A. S. Narizhnaya, A. M. Kuzmenko, and I. A. Gudim, JETP Letters, 93(5), 275-281 (2011).
 - ⁸ A. A. Demidov, and D. V. Volkov, Physics of the Solid State, 53(5), 985-996 (2011).
 - ⁹ A. M. Kuzmenko, D. Szaller, T. Kain, V. Dziom, L. Weymann, A. Shuvaev, and L. N. Bezmaternykh, Physical Review Letters, 120(2), 027203 (2018).
 - ¹⁰ R. Arun Kumar, Journal of Chemistry 2013, Article ID 154862 (2012).
 - ¹¹ C. Chen, T. Sasaki, R. Li, Y. Wu, Z. Lin, Y. Mori, Y. Kaneda, Nonlinear Optical Borate Crystals: Principals and Applications. John Wiley and Sons (2012).
 - ¹² T. Usui, Y. Tanaka, H. Nakajima, M. Taguchi, A. Chainani, M. Oura, S. Shin, N. Katayama, H. Sawa, Y. Wakabayashi, and T. Kimura, Nature Materials 13, 611-618 (2014).
 - ¹³ K. V. Frolov, I. S. Lyubutin, E. S. Smirnova, O. A. Alekseeva, I. A. Verin, V. V. Artemov, and I. A. Gudim, Journal of Alloys and Compounds 671, 545-551 (2016).
 - ¹⁴ Y. Hinatsu, Y. Doi, K. Ito, M. Wakeshima, and A. Alemi, Journal of Solid State Chemistry 172(2), 438-445 (2003).
 - ¹⁵ R. P. Chaudhury, F. Yen, B. Lorenz, Y. Y. Sun, L. N. Bezmaternykh, V. L. Temerov, and C. W. Chu, Physical Review B 80(10), 104424 (2009).
 - ¹⁶ A.I. Pankrats, G.A. Petrakovskii, L.N. Bezmaternykh, O.A. Bayukov, J. Exp. Theor. Phys. 99, 766 (2004).
 - ¹⁷ Y.F. Popov, A.M. Kadomtseva, G.P. Vorob'ev et al. Jetp Lett. 89, 345 (2009).
 - ¹⁸ P. Fischer, V. Pomjakushin, D. Sheptyakov, L. Keller, M. Janoschek, B. Roessli, and D. Velikanov, Journal of Physics: Condensed Matter 18(34), 7975 (2006).
 - ¹⁹ D. K. Shukla, S. Francoual, A. Skaugen, M. V. Zimmermann, H. C. Walker, L. N. Bezmaternykh, and J. Strempfer, Physical Review B 86(22), 224421 (2012).
 - ²⁰ S. Partzsch, J. E. Hamann-Borrero, C. Mazzoli, J. Herrero-Martin, S. Valencia, R. Feyerherm, and J. Geck, Physical Review B 94(5), 054421 (2016).
 - ²¹ J. E. Hamann-Borrero, S. Partzsch, S. Valencia, C. Mazzoli, J. Herrero-Martin, R. Feyerherm, and B. Büchner, Physical Review Letters 109(26), 267202 (2012).
 - ²² C. Ritter, A. Vorotynov, A. Pankrats, G. Petrakovskii, V. Temerov, I. Gudim, and R. Szymczak, Journal of Physics: Condensed Matter 20(36), 365209 (2008).
 - ²³ A. Rogalev, F. Wilhelm, J. Goulon, and G. Goujon. Advanced Instrumentation for X-ray Magnetic Circular Dichroism. In Magnetism and Synchrotron Radiation: Towards the Fourth Generation Light Sources. (Springer International Publishing, 2013), pp. 289-314.
 - ²⁴ F. De Groot, and A. Kotani, Core Level Spectroscopy of Solids. (CRC press, 2008).
 - ²⁵ R. M. Galéra, Y. Joly, A. Rogalev, and N. Binggeli, Journal of Physics: Condensed Matter 20(39), 395217 (2008).
 - ²⁶ F. Bartolomé, J. M. Tonnerre, L. Seve, D. Raoux, J. Chaboy, L. M. Garcia, and C. C. Kao, Physical Review Letters 79(19), 3775 (1997).
 - ²⁷ F. Bartolomé, M. H. Krisch, D. Raoux, and J. M. Tonnerre, Physical Review B 60(19), 13497 (1999).
 - ²⁸ A.P. Menushenkov, V.G. Ivanov, I.V. Shchetinin, D.G. Zhukov, V.P. Menushenkov, I.A. Rudnev, A.A. Ivanov, F. Wilhelm, A. Rogalev, A. and A.G. Savchenko, JETP Letters, 105(1), pp.1-5. (2017).